Desalination and Water Treatment
www.deswater.com
doi: 10.5004/dwt.2023.29700

303 (2023) 121–131
August

Facile synthesis and application of manganese-zinc-cobalt hydrous oxides nanoparticles decorated biochar for decontamination of copper(II) from water

Sana Khalid[a], Rabia Nazir[b,*], Sajid Rashid Ahmad[a], Muhammad Nawaz Chaudhry[c]

[a]*College of Earth and Environmental Sciences, University of the Punjab, Lahore-54000, Pakistan, emails: sanakhalid305@gmail.com (S. Khalid), sajidpu@yahoo.com (S.R. Ahmad)*
[b]*Pakistan Council of Scientific and Industrial Research Laboratories Complex, Ferozepur Road, Lahore-54570, Pakistan, email: rabiapcsir@yahoo.com*
[c]*Department of Environmental Sciences and Policy, Lahore School of Economics (LSE), Lahore-53200, Pakistan, email: muhammadnawazchaudhry@yahoo.com*

Received 23 August 2022; Accepted 17 June 2023

ABSTRACT

The present study evolved around the synthesis of trimetallic composite, manganese-zinc-cobalt hydrous oxides nanoparticles anchored biochar (MZCB) nanocomposite (NC) for decontamination of water and wastewater polluted with Cu(II) ions. The MZCB NC (27 nm) was characterized using Fourier-transform infrared spectroscopy, scanning electron microscopy-energy-dispersive X-ray spectroscopy and powder X-ray diffraction. Batch adsorption studies were performed and the influence of different adsorption parameters (contact time, reaction temperature, solution pH, adsorbent dose and initial adsorbate concentration) were examined. MZCB was found effective in removing (~98%) of Cu(II) in 50 min at pH 5.0 while employing initial dose of 0.1 g and 300 mg·Cu(II)·L^{-1}. The adsorption experimental data was fitted to different adsorption isotherms and kinetic models which exhibited best-fit models to be the general order kinetic model and Redlich–Peterson adsorption model, respectively. The maximum uptake capacity of MZCB with respect to Cu(II) ions was found to be 312.58 mg·g^{-1}.

Keywords: Biochar; Manganese-zinc-cobalt nanocomposite; Kinetic modelling; Adsorption isotherms; Cu(II) removal

1. Introduction

The global paucity of freshwater resources with continuous accelerated human demands for water have intensified the exigency to preserve current water reserves for sustainable growth [1]. The population explosion, industrialization, urbanization and advance agricultural practices have resulted in unchecked release of wastewater loaded with various pollutants into aquatic bodies [2]. Heavy metal pollution has become a serious global issue causing substantial environmental damage and potential health damages to all living beings since these are extremely toxic, persistent, non-biodegradable, and bio-accumulative in nature [3]. Copper [Cu(II)], a highly persistent heavy metal, has widespread applications in the manufacturing of pesticides, fertilizers, paper, automotive and electronic equipment [4]. Though Cu(II) is considered as an essential trace metal for optimal body functioning of living organisms, however, its excess concentrations may pose serious health issues including liver, kidneys, heart, pancreas and brain disorders [5]. Cu(II) toxicity has been found to be linked with incidence of various neurodegenerative disorders such as Alzheimer's, Parkinson's, and Wilson's diseases [6,7]. Thus, the acute toxicity of Cu(II) has urged the requisite for its effective decontamination from environment.

Removal of heavy metals from wastewater is an extremely challenging task. Multitude of water purification

* Corresponding author.

technologies including ion exchange, ozonation, membrane filtration, chemical precipitation, coagulation and flocculation, electro-dialysis, biological treatment, and adsorption have been tested for removal of heavy metals from aqueous solutions [8–13]. Though, adsorption is considered a highly compelling approach for heavy metals decontamination owing to its convenient, efficient, and environmental-friendly nature.

Now days, utilizing agroforestry wastes-based nanoadsorbents for wastewater decontamination has garnered immense focus owing to their widespread availability, low cost and environment-friendly nature [13–15]. Rice straw is produced as an agricultural byproduct during rice harvesting, which is often rejected as solid waste owing to its low economic value, resulting in severe environmental contamination. Thereof, altering the rice straw into biochar for uptake of heavy metals could be a feasible approach for environmental remediation. Biochar has been suggested as a potential adsorbent for the removal of heavy metals from wastewater [16]. However, the amalgamation of metal nanoparticles of interest into biochar matrix may result in enhancement of the specific surface area and surface reactive groups, leading to profound sequestration of heavy metals from aqueous media [17]. There has been conducted extensive research which shows the effective potential of metal/metal oxide biochar-based composites for heavy metals sequestration [18–21]. $KMnO_4$ modified hickory wood biochar removed 34.2 mg·Cu(II)/g of adsorbent [22]. Sodium hydroxide activated biochar was found capable of adsorbing Cu(II) with an adsorption capacity of 17.9 $mg \cdot g^{-1}$ from mixed metal solution [14]. Effective uptake of Cu(II) was also reported by using nano magnesium oxide decorated corncob biochar at pH (5.0), achieving maximum adsorption capacity of 300.2 $mg \cdot g^{-1}$ [13]. Jung et al. [23] reported the superior uptake efficiency of manganese ferrite supported biochar, enabling adsorption of 295.2 mg·Cu(II)/g adsorbent.

Therefore, taking into consideration the plausible effectiveness of biochar and nanomaterials toward viable adsorption of heavy metals from aqueous environment, the present study for the very first time has addressed the synthesis and application of ternary metals hydrous oxides nanoparticles doped rice straw biochar nanocomposite for treatment of Cu(II) polluted water. The prepared nanocomposites (MZCB) exhibited enhanced adsorption capacity for Cu(II), which is much greater than already reported adsorbents (Table 4) with an added advantage of consuming less time to remove Cu(II) ions from aqueous solutions and requiring less stringent conditions for the adsorption, making the adsorption process convenient and cost-effective.

2. Experimental section

All the chemical reagents used in this study were of analytical grade purity. The solutions were prepared in doubly distilled water. Zinc sulfate monohydrate, manganese sulfate monohydrate, sodium hydroxide and nitric acid were purchased from Sigma-Aldrich, Steinheim, Germany, and cobalt chloride hexahydrate and copper chloride dihydrate was obtained from Daejung Chemicals, South Korea. Hydrochloric and sulphuric acids were procured from Pakistan Council of Scientific and Industrial Research (PCSIR) Lahore, Pakistan. All the chemicals were used as received without further purification.

2.1. Synthesis of hydrous metal oxides nanoparticles doped biochar (MZCB)

Rice straw was collected from paddy fields located in Narowal, Pakistan. It was rinsed thoroughly with distilled water for removing adhered dirt and impurities and dried in oven at 80°C for 24 h. The dried rice straw was ground into fine powder and passed through 250 μ sieve. Subsequently, it was pyrolyzed at 600°C for 2 h in oxygen deficient environment to yield biochar. For activation, the fabricated biochar was contacted with 2% sulphuric acid under constant heating and stirring for 90 min. The resultant solution mixture was allowed to cool to room temperature, residues were filtered and washed with distilled water until neutralized.

25 g of acid activated biochar was homogenously dispersed in 1 L distilled water under vigorous stirring. To this suspension, 50 mL of 0.05 M cobalt chloride, zinc sulphate and manganese sulfate solutions were added at slow rate under vigorous stirring, followed by addition of 150 mL of sodium hydroxide (1 M) for precipitation. The resultant suspension was filtered, residue was washed with distilled water and oven dried at 120°C. The as-fabricated biochar composite was ground, stored in air-tight container and labelled as MZCB.

2.2. Characterization of MZCB

Scanning electron microscopy-energy-dispersive X-ray (SEM-EDX) analysis were carried out using Nova NanoSEM 450 field-emission scanning electron microscope (FE-SEM) for examining the surface morphology and chemical composition of MZCB. Attenuated total reflection-Fourier-transform infrared spectroscopy (ATR-FTIR) was studied over a range 4,000–600 cm^{-1} by using Tensor 27 performed to determine the surface functional groups of fabricated biochar composite. The crystalline nature and phase of sample was investigated by using X-ray Diffractometer (D2-Phaser; Bruker, USA).

2.3. Adsorption studies

Batch experiments were conducted to investigate the adsorption of Cu(II) onto MZCB under varying conditions of different experimental parameters (i.e., contact time, temperature, solution pH, adsorbent dose and initial metal ion concentration). For this purpose, stock solution of Cu(II) (1,000 $mg \cdot L^{-1}$) was prepared which was diluted to desired concentrations as per requirement.

For optimizing the process parameters for optimum metal adsorption, batch studies were performed by using 50 mL of Cu(II) ion solution (300–1,000 $mg \cdot L^{-1}$) contained in a conical flask with known adsorbent dosage (0.05–0.3 g). The contents were contacted at 200 rpm for a given time period (2–90 min) at different temperatures (30°C–70°C) and pH (1.0–5.0). The pH of the solution was maintained with the help of 0.1 M HCl and 0.1 M NaOH. Afterwards, the sample suspension was cannula filtered and the residual amount

of Cu(II) in filtrate was analyzed with the help of flame atomic absorption spectrometer (PerkinElmer AAnalyst 200, USA). The percentage removal efficiency (%RE) and the concentration of adsorbate sorbed on adsorbent [adsorption capacity (mg·g^{-1}), q_{exp}] was calculated using Eqs. (1) and (2).

$$\mathrm{RE}(\%) = \left[\frac{C_i - C_f}{C_i}\right] \times 100 \quad (1)$$

$$q_{exp} = \left(C_i - C_f\right) \times \frac{V}{W} \quad (2)$$

where C_i (mg·L^{-1}) and C_f (mg·L^{-1}) are the initial and final concentration of adsorbate in solution, respectively, V (L) is the volume of solution and W (g) is the mass of adsorbent.

3. Results and discussion

3.1. Synthesis of hydrous metal oxides nanoparticles doped biochar

The MZCB was fabricated using rice straw biochar as a template. Rice straw is composed of 45% cellulose, 25% hemicellulose, 15% lignin, and 15% silica. It serves as an appropriate carbonaceous precursor owing to its high lignocellulose content. Biochar was synthesized under slow pyrolysis (600°C) conditions in limited supply of oxygen and volatilization of lignocellulose content of rice straw during carbonization facilitated the development of porous network in biochar. Manganese/zinc/cobalt hydrous oxide nanoparticles were integrated into the porous network of the biochar by using co-precipitation method. The fabricated nanocomposite was characterized using different techniques and investigated for its maximum scavenging capacity as a potential candidate for removal of Cu(II), a potential contaminant in industrial effluents.

3.2. Characterization of hydrous metal oxides nanoparticles doped biochar

3.2.1. Fourier-transform infrared spectroscopy

FTIR spectrum of MZCB (Fig. 1a) presents a typical spectrum of biochar equipped with major bands referring to C, H, O bonds with some peaks indicative of silica which is characteristic of rice straw biochar. The –OH groups due to adsorbed water molecules in the nanocomposite generated signals of weak intensity in the spectra at 3,353 cm^{-1} [24]. The peaks evidenced at 2,325; 2,085 and 2,000 cm^{-1} correspond to C≡C stretching and the band at 1,565 cm^{-1} is attributed to –COO stretching vibrations [25]. The appearance of peak at 1,365 cm^{-1} is related to –CH_2 or –CH_3 groups [26]. The signal at 1,023 cm^{-1} attributes to C–O stretching and C–OH bending [25,26], while the peak at 786 cm^{-1} is related to Si–O–Si bond [27].

3.2.2. Scanning electron microscopy-energy-dispersive X-ray spectroscopy

SEM-EDX analysis was conducted for investigating surface morphological attributes and elemental composition of MZCB. SEM micrograph along with EDX mapping and elemental composition of MZCB is presented in Figs. 1b and c, respectively. Fig. 1b displays aggregated biochar particles (black) with homogenous deposition of hydrous metal oxide nanoparticles (white) on its surface. The image of MZCB exhibits that manganese, zinc and cobalt hydrous oxide nanoparticles have fluffy texture,

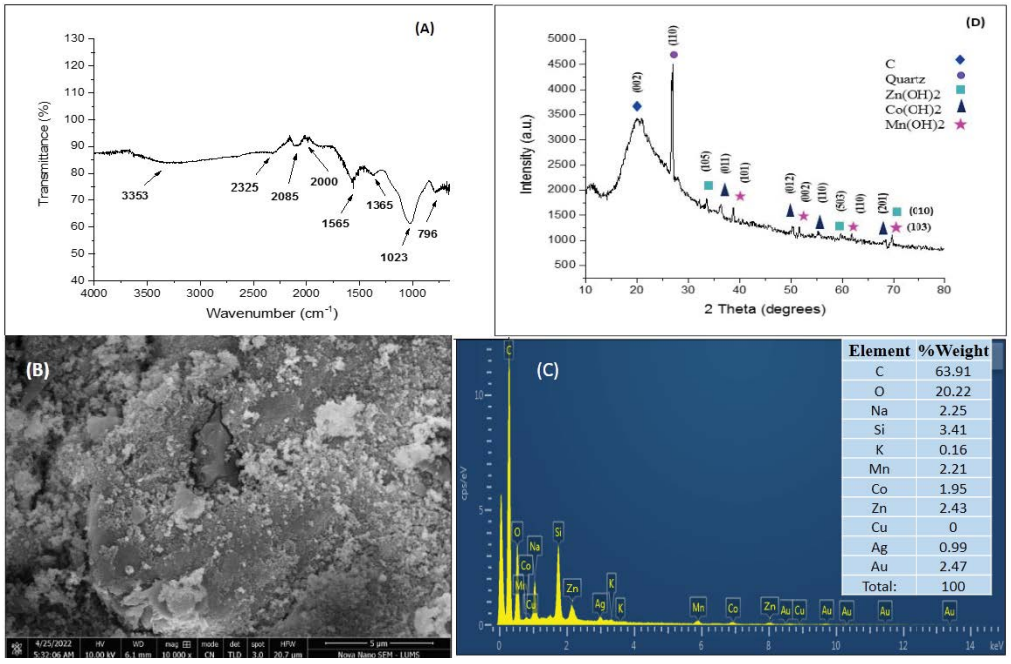

Fig. 1. (a) Fourier-transform infrared spectroscopy, (b) scanning electron microscopy micrograph, (c) energy-dispersive X-ray spectroscopy and (d) X-ray diffractogram of MZCB.

and present in agglomerated form above the biochar matrix. These findings are in accordance with the previous studies [25]. Elemental composition is affirmed by EDX spectrum, presented in Fig. 1c. Peaks of carbon (C) and oxygen (O) are highly evident in the spectrum, with weight percentages of 63.91% and 20.22%, respectively owing to the biochar and presence of oxygen bearing functional groups in the nanocomposite, while Si is present in 3.41% weight ratio, which is one of the dominant components of rice straw. The quantitative data displays occurrence of Co (1.95%), Zn (2.43%) and Mn (2.21%) metals in the nanocomposite. A small quantity of K is probably present due to its occurrence in rice straw biomass while Na is present due to NaOH used for co-precipitation.

3.2.3. X-ray diffraction and Brunauer–Emmett–Teller analysis

Fig. 1d represents the powder X-ray diffractogram of MZCB. The diffraction peak plane hkl (002) relates to C and the peak broadness of which accredits the amorphous nature of biochar [28]. The sharp peak appearing at hkl (110) corresponds to quartz (main phase of rice straw charcoal), which is in good accordance with JCPDS card no. 46-1045 [27,29]. The peak planes referring to hkl values of (011), (012), (110) and (201) conform to $Mn(OH)_2$ (JCPDS card no. 73-1604) [30], while peaks corresponding to planes values of (101), (002), (110) and (103) are related to $Co(OH)_2$, which matches well with JCPDS card no. 45-0031 [31,32]. The diffraction peak planes ascribing to hkl values of (105), (503) and (010) are indexed to $Zn(OH)_2$, which is in good agreement with JCPDS card no. 38-0356 [33]. The low peak intensity of metal hydroxides ascribes to their poor crystalline nature owing to smaller crystallite size suggesting the formation of nanocomposite [25]. The particle size as calculated from the Debye Scherrer equation comes out to be 27 nm confirming the formation of nanocomposite.

The obtained N_2 adsorption isotherms at 77 K for MZCB is presented in Fig. 2. The total pore volume, pore diameter and Brunauer–Emmett–Teller specific surface area for MZCB are 1.85×10^{-3} $cm^3 \cdot g^{-1}$, <2.6 nm and 29.52 $m^2 \cdot g^{-1}$, respectively.

3.3. Adsorption studies

MZCB was investigated for its efficacy against Cu(II) removal from aqueous solutions in batch mode as function of varying experimental conditions (contact time, temperature, solution pH, adsorbent dose and initial metal ion concentration).

3.3.1. Effect of contact time and adsorption kinetics

Contact time is an imperative function to be studied during the adsorption experiments [34,35]. The influence of contact time on the adsorption of Cu(II) by adsorbent (Fig. 3a) was investigated by agitating 50 mL of Cu(II) ion solution (500 $mg \cdot L^{-1}$) in conical flask with 0.1 g of adsorbent at room temperature and initial solution pH 4.0 for different contact period (2–90 min). In the initial phase, Cu(II) sorption occurred very rapidly due to bulk number of vacant

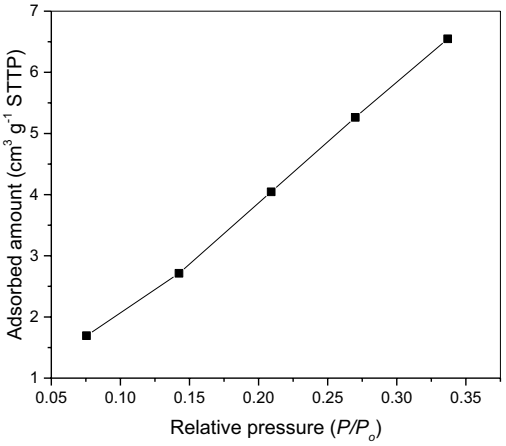

Fig. 2. N_2 adsorption isotherms for MZCB at 77 K.

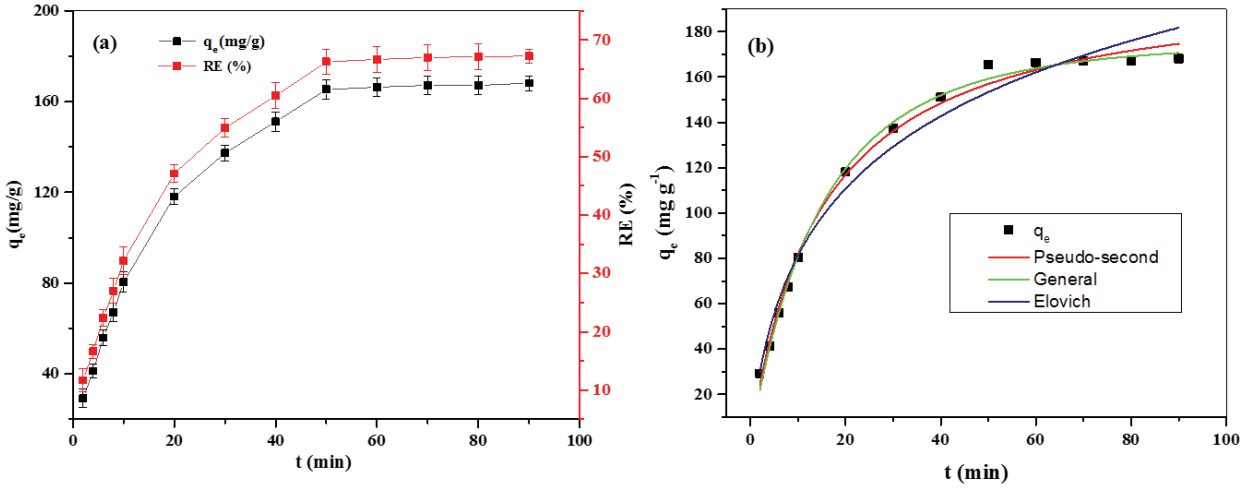

Fig. 3. Effect of variation of time to MZCB for Cu(II) adsorption (a), and fitting of kinetic models to MZCB for adsorption of Cu(II) (b).

reactive sites on the surface of nanocomposite enabling binding with metal ions, leading to swift reaction rate. The Cu(II) ions uptake on MZCB augmented with increment in contact time until equilibrium stage was attained at 50 min with RE of 66.5% (q_e = 166.14 mg·g^{-1}). Other studies reported much higher time for uptake of Cu(II) ions, that is, 24 and 10 h by use of magnesium oxide nanoparticles doped corn cob biochar and modified magnetic rice straw biochar, respectively [13,36].

Adsorption kinetics explains the sorption rate of solute onto the adsorbent and is a highly prominent function for evaluating the removal efficiency of an adsorbent and getting insight into the adsorption phenomena. Different kinetics models (pseudo-first-order [35], pseudo-second-order [37], general order [38] and Elovich [39]) in non-linear form mentioned in Eqs. (3)–(6), respectively, were fitted to experimental data (Fig. 3b).

$$q_t = q_e\left[1-\exp\left(-k_1\cdot t\right)\right] \tag{3}$$

$$q_t = \frac{t\cdot k_2\cdot q_e^2}{1+t\cdot k_2\cdot q_e} \tag{4}$$

$$q_t = q_e - \frac{q_e}{\left[k_3\cdot\left(q_e^{(n-1)}\right)\cdot t\cdot\left(n-1\right)+1\right]^{(1/(1-n))}} \tag{5}$$

$$q_t = \frac{1}{b}\left[\ln\left(a\cdot b\cdot t+1\right)\right] \tag{6}$$

where q_t (mg·g^{-1}) is the concentration of adsorbent at time t (min), q_e (mg·g^{-1}) is the concentration at equilibrium, k_1 (min^{-1}) and k_2 (g·mg^{-1}·min^{-1}) and k_3 (min^{-1}(g·mg^{-1})$^{n-1}$) are the rate constants for pseudo-first, pseudo-second and general orders, respectively, a (mg·g^{-1}·min^{-1}) is the initial rate of adsorption, b (g·mg^{-1}) is the desorption constant and n is the kinetic sorption order (n could be an integer or a fractional value).

The best fitting of model was assumed from highest R^2, lowest reduced chi-square and standard deviation values, and close accordance between experimental ($q_{e,\exp}$) and calculated ($q_{e,\text{cal}}$) adsorption capacity. The adoption data did not converge to pseudo-first-order kinetic model (data and model fitting is not presented in Fig. 3b), while other three models registered good-fitting to the experimental data. However, general order kinetic model exhibited best-fitting to the experimental sorption data as justified by highest R^2 (>0.995) and close accordance between $q_{e,\exp}$ (168.15 mg·g^{-1}) and $q_{e,\text{cal}}$ (176.0 mg·g^{-1}) adsorption capacities. The goodness of fitting of adsorption data to general order kinetic model indicates that there is a shift in orders during the course of adsorption process [40]. In case of Elovich model, the higher value of '*a*' denoted that the initial adsorption rate was high while the lower value of '*b*' indicated lower desorption rate [41]. In addition, higher value of '*a*' and lower value of '*b*' obtained also implicate that adsorbent possesses bulk density of reactive sorption sites and high electron donor potential [42]. The kinetic modelling parameters are given in Table 1.

3.3.2. Effect of temperature and thermodynamic parameters

To examine the impact of temperature, a set of batch experiments were performed by changing temperature from 30°C–70°C, while keeping the other parameters [contact time (50 min), adsorbent dose (0.1 g), Cu(II) ion concentration (50 mL of 500 mg·L^{-1}) and pH (4.0)] constant. Fig. 4a displays the influence of temperature variation on the adsorption of Cu(II) onto MZCB from aqueous solution. The % metal sorption efficacy improves with increase in reaction temperature due to thermal activation of Cu(II) ions which results in fast movement of metal ions, thus leading to high sorption performance [43]. The metal uptake increased incrementally with rise in temperature up to 50°C, thereafter further increase in temperature recorded negligible increase in sorption since equilibrium phase was attained. The %RE increased from 66.55% to 73.07% (q_e, 166.40–183.68 mg·g^{-1}) with increment in temperature from 30°C to 70°C. Moreover, the desorption of bounded metal ions may happen at elevated temperatures which drops the removal efficiency of fabricated nanocomposite.

Thermodynamic parameters, that is, standard fee energy change ($\Delta G°$), standard enthalpy change ($\Delta H°$) and standard entropy change ($\Delta S°$), are calculated using the following equations:

$$\Delta G = -RT\ln K_C \tag{7}$$

$$\text{where, } K_C = \frac{C_S}{C_e} \tag{8}$$

$$\ln K_C = \left(\frac{\Delta S°}{R}\right) - \left(\frac{\Delta H°}{RT}\right) \tag{9}$$

where K_C, C_S and C_e are equilibrium constant, equilibrium concentration of the metal sorbed on the adsorbent in mg·L^{-1}, and equilibrium concentration of metal in the solution in mg·L^{-1}. R is ideal gas constant which value is

Table 1
Adsorption kinetics model fitting parameters

Model	Parameter	Cu(II)
Pseudo-second-order	k_2 (min^{-1})	3.31 × 10^{-4}
	$q_{e,\text{cal}}$ (mg·g^{-1})	203.4
	adjR^2	0.993
	Reduced chi-square	19.05
General order	k_3 (min^{-1})	0.015
	N	1.297
	$q_{e,\text{cal}}$ (mg·g^{-1})	176.0
	adjR^2	0.996
	Reduced chi-square	12.56
Elovich	a (mg·g^{-1}·min^{-1})	20.29
	b (g·mg^{-1})	0.02
	adjR^2	0.977
	Reduced chi-square	36.68

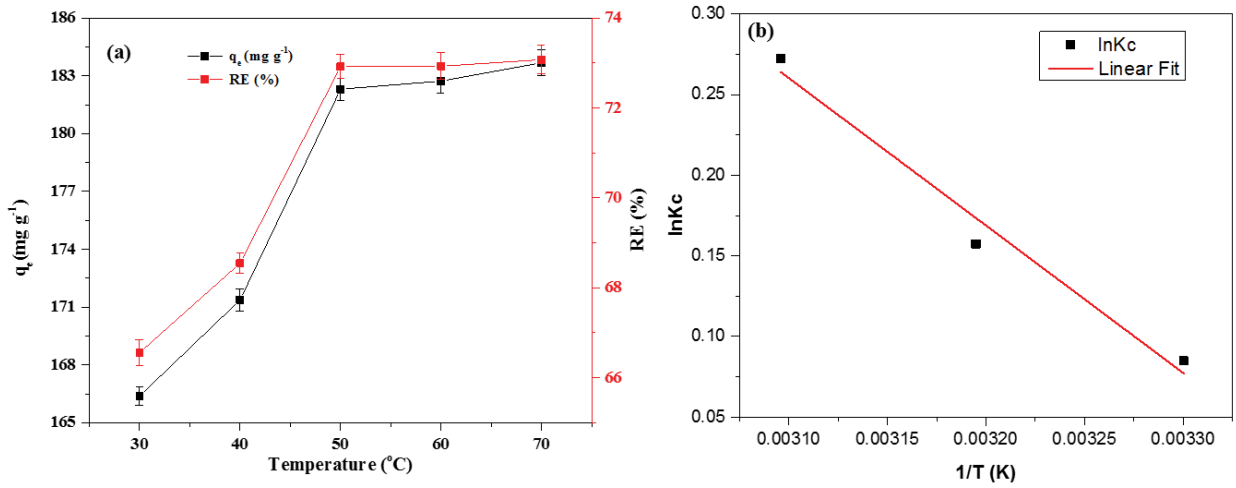

Fig. 4. Effect of variation of temperature (a) and its application of thermodynamic model (b) on adsorption of Cu(II) onto MZCB.

8.314 J·mol^{-1}·K^{-1} and T is the adsorption temperature in Kelvin.

The plot of lnK_C vs. T^{-1} for the adsorption of Cu on nanocomposite (Fig. 4b) is used to calculate $\Delta H°$ and $\Delta S°$ from slope and intercept, respectively (Table 2). The values show that the adsorption of Cu(II) on to MZCB is spontaneous ($-\Delta G°$) and endothermic ($+\Delta H°$) but points to disorderness around the adsorbent surface owing to strong affinity of metal with adsorbent as reflected by $+\Delta S°$ value [44–48]. The increase in randomness at aqueous/solid interface during the adsorption process can be attributed to the fact that adsorbed water molecules (that are displaced by the adsorbate species when metals are transformed from aqueous to solid phase) attain more translational energy as compared to energy lost by adsorbate ions as a result of associative and dissociative mechanisms [46]. The associative and dissociative are 2 mechanisms related to $\Delta S°$ values. If $\Delta S°$ value is greater than −10, the dominant mechanism would be dissociative. In the present study, $\Delta S°$ value for Cu(II) ions was higher than −10 (J·mol^{-1}·K^{-1}), which is indicative of the dissociative mechanism. This exhibited that the freely existing Cu(II) metal ions ratio to the ions interacting with MZCB surface is greater than the adsorbed state [49].

3.3.3. Effect of pH

The pH of solution is a significant experimental parameter, which is highly necessary to be investigated in adsorption studies as it controls the uptake of metal ions onto the adsorbent surface. In order to determine the effect of pH on Cu(II) ion adsorption, batch experiments were performed at various pH values ranging from 1.0 to 5.0 and experiments at pH > 5.0 were not conducted due to formation of insoluble precipitates of copper. For this, 50 mL of Cu(II) solution (500 mg·L^{-1}) was agitated for 50 min with 0.1 g of adsorbent at temperature (50°C) and altering pH levels (1.0–5.0). The data is presented in Fig. 5a.

In pH range of 3.0–4.0, Cu^{2+} and $CuOH^{+}$ ions are the most prevalent species of Cu(II); whereas at pH (>5.0) Cu(II) exists as insoluble precipitates of $Cu(OH)_2$ [50]. Fig. 5a represents the impact of pH variation on the removal of Cu(II)

Table 2
Thermodynamic parameters' values for adsorption of Cu(II) on MZCB

Nano-adsorbents	T (K)	K_C	$\Delta G°$ (kJ·mol^{-1})	$\Delta H°$ (kJ·mol^{-1})	$\Delta S°$ (kJ·mol^{-1}·K^{-1})
MZCB	302	1.09	−0.21	7.60	0.03
	313	1.17	−0.41		
	323	1.31	−0.73		

onto MZCB from aqueous media. The % removal of Cu(II) enhances with increase in pH and the maximum adsorption of Cu(II) (185.95 mg·g^{-1}) was recorded at pH 5.0 with %RE of 74.18%. At pH < $pH_{(PZC)}$ (i.e., 3.67 (Fig. 5b), the adsorbent surface becomes protonated due to presence of excessive H^+ ions in the aqueous solution which hinder the binding of Cu(II) on adsorbents' surface due to existence of electrostatic repulsion between H^+ and metal ions. With the increment in pH > $pH_{(PZC)}$, the character of oxygen bearing surface functionalities (COOH, OH) present on the surface of nanocomposite alters and the surface gets anionic charge which results in electrostatic attraction between negatively charged adsorbents' surface and Cu(II) ionic species, leading to high metal uptake activity [13]. The similar response was evidenced in the present study in which low uptake of Cu(II) ions onto the fabricated nanocomposite was observed in acidic medium and began to increase with increment in pH and highest removal efficiency was recorded at pH 5.0.

3.3.4. Effect of adsorbent dose

The effect of adsorbent dose on Cu(II) removal was examined in batch studies by altering its dose (0.05–0.3 g) at optimum time (50 min), temperature (50°C), pH (5.0) and using 500 mg·L^{-1} of Cu(II) ions solution. It is evident from the graph (Fig. 6) that with variation in adsorbent dosage from 0.05 to 0.1 g there is a noticeable increment in % removal efficiency from 38.77% to 74.18% Cu(II) and further

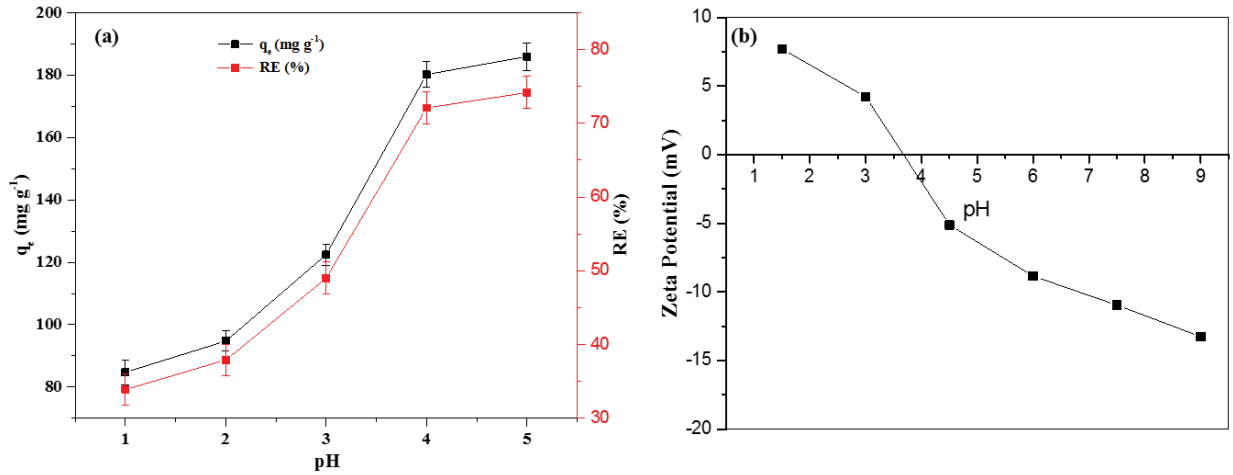

Fig. 5. Effect of variation of initial pH on adsorption of Cu(II) onto MZCB (a), and pH_{PZC} for MZCB (b).

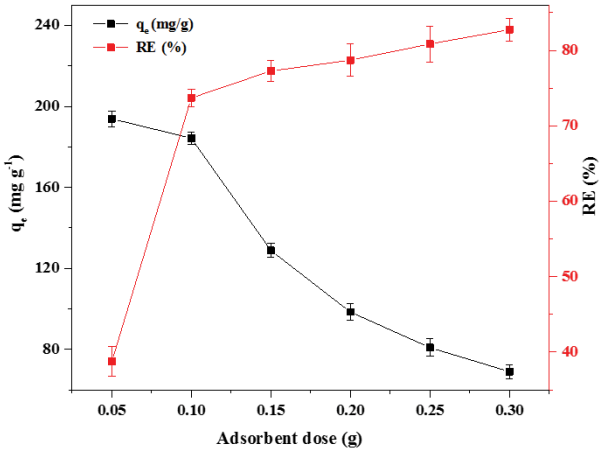

Fig. 6. Effect of variation of adsorbent dose on adsorption of Cu(II) onto MZCB.

increment in adsorbent dose up to 0.3 g registered not significant increase in Cu(II) removal efficiency (i.e., 82.7%).

This enhancement in % RE of Cu(II) is ascribed to increase in the bulk density of reactive sites and surface functionalities for binding of metal ions. The maximum adsorption capacity was noted at 0.1 g adsorbent dose, so it is considered as optimal dose for adsorption of Cu(II). However, for surge in adsorbent dosage above the 0.1 g, the substantial decline in adsorption capacity was noticed. This is credited to the fact that increase in adsorbent dose amplifies the number of vacant active sites which in the beginning encourages the scavenging potential, but the sorption activity compromised beyond the optimal dose because massive number of active sorption sites are left unbounded because the adsorbent dose is increased at fixed concentration of metal ions [15].

3.3.5. Effect of initial metal ion concentration and adsorption isotherm

The effect of initial Cu(II) ion concentration was investigated by altering metal ion concentrations in the range of 300–1,000 mg·L^{-1}, while maintaining the rest of adsorption parameters constant as optimized in the preceding experiments. At lower Cu(II) ions concentration, the concentration of metal ions occurring in the aqueous media is low that enabled the interaction of maximum number of metal ions with vacant binding sites for uptake, promoting 97.30% metal adsorption at 300 mg·L^{-1}. As the metal ion concentration increased, metal ions available in the system enhanced resulting in competition between them for binding to active sites. As a result, the large number of metal ions would remain un-bounded because of the saturation of reactive sites [14,21]. The % RE of biochar nanocomposite was decreased from 97.30% to 46.09% with increase in metal ion concentration from 300–1,000 mg·L^{-1} (Fig. 7a).

To get deep insight into the nature of sorption system, it is required to conduct the study of equilibrium isotherms. Langmuir model proposes that adsorption process takes place on homogenous sites via monolayer adsorption with no interaction between adsorbate–adsorbent molecules [51].

$$q_e = \frac{q_m \cdot K_l \cdot C_e}{1 + K_l \cdot C_e} \tag{10}$$

where K_l is Langmuir constant (L·mg^{-1}) associated to the energy of sorption and q_m is the maximum adsorption capacity of the adsorbent (mg·g^{-1}), C_e is the concentration of adsorbate at equilibrium and q_e represents the sorption capacity at equilibrium (mg·L^{-1}). The K_l can be employed for calculating the Langmuir partitioning factor (dimensionless constant), R_L, using the following equation:

$$R_L = \frac{1}{\left(1 + K_l \cdot C_0\right)} \tag{11}$$

where C_0 represents the initial concentration of adsorbate (mg·L^{-1}). The value of R_L predicts about the nature of sorption process to be like; if $R_L = 1$ (linear); $R_L = 0$ (irreversible); $0 < R_L < 1$ (favorable) and $R_L > 1$ (unfavorable) [52].

Freundlich isotherm addresses heterogeneity of adsorbent surface and obeys multilayer adsorption of adsorbate molecules on adsorbent surface [9].

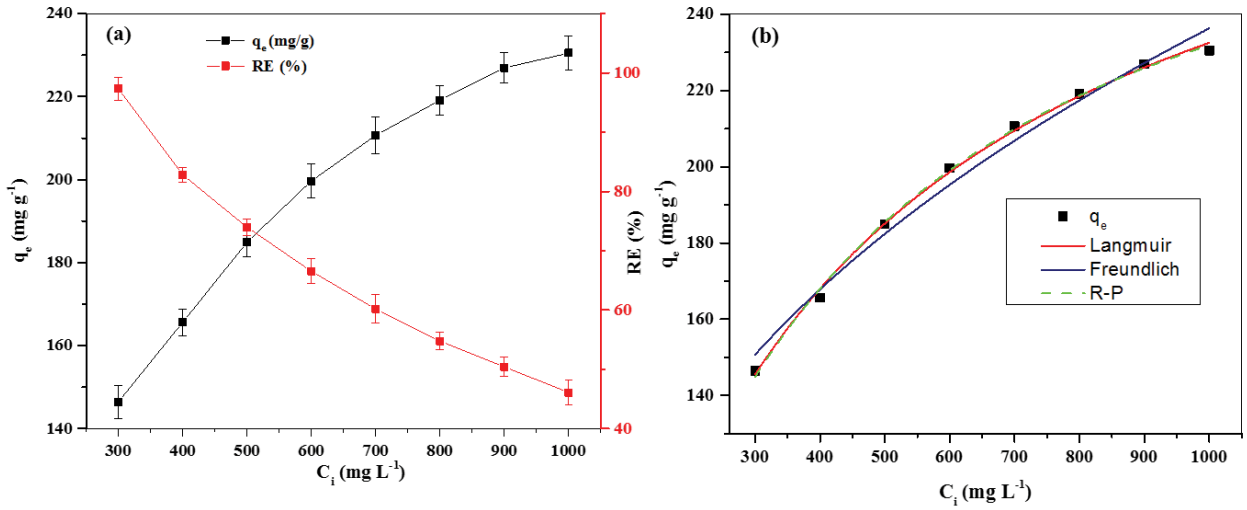

Fig. 7. Effect of variation of initial metal concentration to MZCB for adsorption of Cu(II) (a), and fitting of isotherm models to MZCB for adsorption of Cu(II) (b).

$$q_e = K_F\left(C_e^{1/n_F}\right) \tag{12}$$

where K_F ((mg·g^{-1})(L·mg^{-1})$^{1/n}$) represents the intensity of sorption and n_F is the Freundlich dimensionless constants which measures the deviation of sorption process from linearity.

Redlich–Peterson (R-P) isotherm is a 3 parameter model which delineates the homogenous and heterogeneous behaviors of sorption process by incorporating the features of Langmuir and Freundlich models [53].

$$q_e = \frac{K_R \cdot C_e}{\left(1 + a \cdot C_e^g\right)} \tag{13}$$

where K_R is the R-P constant (L·g^{-1}), a is R-P isotherm constant (L·mg^{-1}), and g is an exponent which has value in the range of 0 to 1. C_e is the concentration of adsorbate at equilibrium (mg·L^{-1}) and q_e is the adsorption capacity at equilibrium (mg·g^{-1}).

The Langmuir, Freundlich and R-P isotherm models (non-linearized) were fitted to the experimental data. Table 3 lists the isotherm model parameters, which delivers that the Langmuir and R-P isotherm models are well consistent with experimental data (Fig. 7b) as compared to Freundlich isotherm model. However, the R-P model holds best for adsorption of Cu(II) on MZCB due to highest R^2 (0.998) and lowest reduced chi-square (Table 3).

The K_l value obtained from Langmuir isotherm model ranging between 0–1 suggested a good interaction between adsorbent and adsorbate molecules. The value of R_L obtained is 0.41, which is less than unity, indicating that the adsorption of Cu(II) ions on MZCB surface was favorable. The favorability of adsorption of Cu(II) ions on nanocomposite was also affirmed by n_F value (2.67) obtained from Freundlich isotherm model which fall in the range from (1–10). The $1/n_F$ value (0.37) indicated the surface heterogeneity of MZCB. The R-P exponent 'g' value is approaching unity (i.e., 0.98), signifying that R-P is reducing to

Table 3
Adsorption isotherm model fitting parameters

Model	Parameter	Cu(II)
Langmuir	K_l (L·mg^{-1})	0.029
	q_m (mg·g^{-1})	312.58
	R_L	0.41
	adjR^2	0.997
	Reduced chi-square	2.33
Freundlich	K_F (mg·g^{-1}(mg·L^{-1})$^{-1/nF}$)	17.88
	n_F	2.67
	adjR^2	0.981
	Reduced chi-square	16.72
Redlich–Peterson	K_R (L·g^{-1})	0.834
	g	0.98
	a (L·mg^{-1})	1.8×10^{-3}
	adjR^2	0.998
	Reduced chi-square	2.15

Langmuir isotherm. This suggests that the uptake of Cu(II) ions occurs through monolayer adsorption on the heterogeneous surface of MZCB having relatively equivalent binding energies [17,54]. These findings are in good agreement with previous findings where adsorption of metal ions on various hybrid nanocomposite matrices obeyed Langmuir isotherm [20,43].

The results show that under optimal conditions of pH (5.0), contact time of 50 min, adsorbent dosage of 0.1 g, room temperature and baseline metal concentration of (300–1,000) mg·L^{-1}, the maximum Langmuir sorption capacity (q_m) of MZCB for Cu(II) was 312.58 mg·g^{-1}. It can be seen from Table 4 that MZCB demonstrated enhanced adsorption capacity for Cu(II) than most of the adsorbents reported in the earlier studies. In comparison with commercial adsorbents, employment of MZCB in wastewater purification signifies a more economically viable and environment

Table 4
Comparison of Cu(II) adsorption potential of various adsorbents

Adsorbent	Adsorption capacity ($mg \cdot g^{-1}$)	Adsorption kinetic and isotherm models	References
Modified magnetic rice straw biochar	85.93	Pseudo-second, Langmuir	[36]
Al/Mn dual layered oxide anchored crab shell biochar	66.23	Pseudo-second, Langmuir	[55]
Potassium ferrate modified wheat stalk biochar	46.85	Langmuir	[20]
Fe_3O_4 impregnated calcium alginate functionalized coconut shell biochar	40.42	Pseudo-second, Langmuir	[54]
Calcium hydroxyapatite modified *Undaria pinnatifida* roots derived biochar	99.01	Pseudo-second, Langmuir	[43]
Nano MgO incorporated corncob biochar	300.2	Pseudo-second, Langmuir	[13]
Manganese ferrite supported biochar	295.2	Pseudo-second, Sips	[23]
MnO_2 nanoparticles loaded biochar	142.02	Pseudo-second, Langmuir	[21]
MnO_2/Mn_3O_4 supported hickory wood biochar	34.2	Pseudo-second, Redlich–Peterson	[22]
Fe_3O_4 decorated pectin nanocomposite	48.99	Pseudo-second, Freundlich, Langmuir	[15]
Fe_3O_4 functionalized kelp (microalgae) biochar	69.37	Langmuir	[17]
Fe_3O_4 functionalized Hijikia (microalgae) biochar	63.52	Langmuir	[17]
MZCB	312.58	General pseudo, Redlich–Peterson	Current studies

friendly alternative since it provides an innovational and green perspective of reutilizing the agricultural waste of low economic value to fabricate plausibly efficient nanoadsorbent, which has addressed the dual benefits of reduction in environmental pollution by solid waste management and additional cost saving which might incur on their disposal. The application of MZCB in environmental cleanup effusively fulfils the objectives of sustainable economy which entails to minimize waste generation by their recycling and reuse. Moreover, utilizing biochar as an alternative to commercial adsorbents permits to evade the environmental impacts of industrial activities caused during their manufacturing. The fabricated trimetallic hydrous oxide biochar nanocomposite (MZCB) registered profound Cu(II) removal from aqueous system in addition to being less time consuming and requiring less stringent conditions for the adsorption. Thus, MZCB can be used as a potential nanoadsorbent for the abatement of heavy metals from aqueous environments.

4. Conclusion

In the present study, the application of MZCB for adsorption of Cu(II) was investigated and batch studies were conducted for optimizing the adsorption process parameters. Superior uptake (~98%) of Cu(II) was achieved by using MZCB at pH 5.0 and 50°C in just 50 min while using 0.1 g of adsorbent. Several adsorption kinetic and thermodynamic models were applied to experimentally calculated data which points to spontaneous removal of Cu(II) from the system while obeying general order kinetics and R-P adsorption model. The results demonstrated that MZCB can sorb Cu(II) in less time with profound removal capacity (312.58 $mg \cdot g^{-1}$).

References

[1] A. Mosa, A. El-Ghamry, P. Trüby, M. Omar, B. Gao, A. Elnaggar, Y. Li, Chemo-mechanical modification of cottonwood for Pb^{2+} removal from aqueous solutions: sorption mechanisms and potential application as biofilter in drip-irrigation, Chemosphere, 161 (2016) 1–9.
[2] X. Garcia, D. Pargament, Reusing wastewater to cope with water scarcity: economic, social and environmental considerations for decision-making, Resour. Conserv. Recycl., 101 (2015) 154–166.
[3] R. Xiao, S. Wang, R. Li, J.J. Wang, Z. Zhang, Soil heavy metal contamination and health risks associated with artisanal gold mining in Tongguan, Shaanxi, China, Ecotoxicol. Environ. Saf., 141 (2017) 17–24.
[4] R.F. Mikesell, The World Copper Industry: Structure and Economic Analysis, RFF Press, New York, USA, 2013.
[5] O. Ademuyiwa, R. Agarwal, R. Chandra, J.R. Behari, Effects of sub-chronic low-level lead exposure on the homeostasis of copper and zinc in rat tissues, J. Trace Elem. Med. Biol., 24 (2010) 207–211.
[6] W. Cerpa, L. Varela-Nallar, A.E. Reyes, A.N. Minniti, N.C. Inestrosa, Is there a role for copper in neurodegenerative diseases?, Mol. Aspects Med., 26 (2005) 405–420.
[7] S. Rivera-Mancía, I. Pérez-Neri, C. Ríos, L. Tristán-López, L. Rivera-Espinosa, S. Montes, The transition metals copper and iron in neurodegenerative diseases, Chem. Biol. Interact., 186 (2010) 184–199.
[8] A. Kaya, C. Onac, H.K. Alpoguz, A novel electro-driven membrane for removal of chromium ions using polymer inclusion membrane under constant DC electric current, J. Hazard. Mater., 317 (2016) 1–7.
[9] J.A. Korak, R. Huggins, M. Arias-Paic, Regeneration of pilot-scale ion exchange columns for hexavalent chromium removal, Water Res., 118 (2017) 141–151.
[10] U. Habiba, T.A. Siddique, T.C. Joo, A. Salleh, B.C. Ang, A.M. Afifi, Synthesis of chitosan/polyvinyl alcohol/zeolite composite for removal of methyl orange, Congo red and chromium(VI) by flocculation/adsorption, Carbohydr. Polym., 157 (2017) 1568–1576.
[11] B. Fraser, M. Pritzker, R. Legge, Development of liquid membrane pertraction for the removal and recovery of

chromium from aqueous effluents, Sep. Sci. Technol., 29 (1994) 2097–2116.
[12] A.S. Abyaneh, M.H. Fazaelipoor, Evaluation of rhamnolipid (RL) as a biosurfactant for the removal of chromium from aqueous solutions by precipitate flotation, J. Environ. Manage., 165 (2016) 184–187.
[13] Y. Deng, X. Li, F. Ni, Q. Liu, Y. Yang, M. Wang, T. Ao, W. Chen, Synthesis of magnesium modified biochar for removing copper, lead and cadmium in single and binary systems from aqueous solutions: adsorption mechanism, Water, 13 (2021) 599, doi: 10.3390/w13050599.
[14] Z. Ding, X. Hu, Y. Wan, S. Wang, B. Gao, Removal of lead, copper, cadmium, zinc, and nickel from aqueous solutions by alkali-modified biochar: batch and column tests, J. Ind. Eng. Chem., 33 (2016) 239–245.
[15] J.-L. Gong, X.-Y. Wang, G.-M. Zeng, L. Chen, J.-H. Deng, X.-R. Zhang, Q.-Y. Niu, Copper(II) removal by pectin–iron oxide magnetic nanocomposite adsorbent, Chem. Eng. J., 185 (2012) 100–107.
[16] R. Mohadi, N.R. Palapa, T. Taher, P.M.S.B.N. Siregar, N. Juleanti, A. Wijaya, A. Lesbani, Removal of Cr(VI) from aqueous solution by biochar derived from rice husk, Commun. Sci. Technol., 6 (2021) 11–17.
[17] E.-B. Son, K.-M. Poo, J.-S. Chang, K.-J. Chae, Heavy metal removal from aqueous solutions using engineered magnetic biochars derived from waste marine macro-algal biomass, Sci. Total Environ., 615 (2018) 161–168.
[18] R. Xiao, J.J. Wang, R. Li, J. Park, Y. Meng, B. Zhou, S. Pensky, Z. Zhang, Enhanced sorption of hexavalent chromium [Cr(VI)] from aqueous solutions by diluted sulfuric acid-assisted MgO-coated biochar composite, Chemosphere, 208 (2018) 408–416.
[19] Y. Zhang, N. Liu, Y. Yang, J. Li, S. Wang, J. Lv, R. Tang, Novel carbothermal synthesis of Fe, N co-doped oak wood biochar (Fe/N-OB) for fast and effective Cr(VI) removal, Colloids Surf., A, 600 (2020) 124926, doi: 10.1016/j.colsurfa.2020.124926.
[20] J. Yan, X. Zuo, S. Yang, R. Chen, T. Cai, D. Ding, Evaluation of potassium ferrate activated biochar for the simultaneous adsorption of copper and sulfadiazine: competitive versus synergistic, J. Hazard. Mater., 424 (2022) 127435, doi: 10.1016/j.jhazmat.2021.127435.
[21] L. Zhou, Y. Huang, W. Qiu, Z. Sun, Z. Liu, Z. Song, Adsorption properties of nano-MnO_2–biochar composites for copper in aqueous solution, Molecules, 22 (2017) 173, doi: 10.3390/molecules22010173.
[22] H. Wang, B. Gao, S. Wang, J. Fang, Y. Xue, K. Yang, Removal of Pb(II), Cu(II), and Cd(II) from aqueous solutions by biochar derived from $KMnO_4$ treated hickory wood, Bioresour. Technol., 197 (2015) 356–362.
[23] K.-W. Jung, S.Y. Lee, Y.J. Lee, Facile one-pot hydrothermal synthesis of cubic spinel-type manganese ferrite/biochar composites for environmental remediation of heavy metals from aqueous solutions, Bioresour. Technol., 261 (2018) 1–9.
[24] C. Aguilar, R. García, G. Soto-Garrido, R. Arriagada, Catalytic wet air oxidation of aqueous ammonia with activated carbon, Appl. Catal., B, 46 (2003) 229–237.
[25] U. Kamran, S.-J. Park, MnO_2-decorated biochar composites of coconut shell and rice husk: an efficient lithium ions adsorption-desorption performance in aqueous media, Chemosphere, 260 (2020) 127500, doi: 10.1016/j.chemosphere.2020.127500.
[26] X.-J. Liu, M.-F. Li, S.K. Singh, Manganese-modified lignin biochar as adsorbent for removal of methylene blue, J. Mater. Res. Technol., 12 (2021) 1434–1445.
[27] D. Mohan, K. Abhishek, A. Sarswat, M. Patel, P. Singh, C.U. Pittman Jr., Biochar production and applications in soil fertility and carbon sequestration–a sustainable solution to crop-residue burning in India, RSC Adv., 8 (2018) 508–520.
[28] T. Chen, R. Liu, N.R. Scott, Characterization of energy carriers obtained from the pyrolysis of white ash, switchgrass and corn stover—biochar, syngas and bio-oil, Fuel Process. Technol., 142 (2016) 124–134.
[29] X. Xu, X. Hu, Z. Ding, Y. Chen, Effects of copyrolysis of sludge with calcium carbonate and calcium hydrogen phosphate on chemical stability of carbon and release of toxic elements in the resultant biochars, Chemosphere, 189 (2017) 76–85.
[30] X. Zhang, Y. Qian, Y. Zhu, K. Tang, Synthesis of Mn_2O_3 nanomaterials with controllable porosity and thickness for enhanced lithium-ion batteries performance, Nanoscale, 6 (2014) 1725–1731.
[31] T. Zhou, Z. Cao, X. Tai, L. Yu, J. Ouyang, Y. Li, J. Lu, Hierarchical $Co(OH)_2$ dendrite enriched with oxygen vacancies for promoted electrocatalytic oxygen evolution reaction, Polymers, 14 (2022) 1510, doi: 10.3390/polym14081510.
[32] R. Shokrani-Havigh, Y. Azizian-Kalandaragh, Preparation of cobalt hydroxide and cobalt oxide nanostructures using ultrasonic waves and investigation of their optical and structural properties, J. Optoelectron. Adv. Mater., 19 (2017) 283–288.
[33] F.V. Molefe, L.F. Koao, B.F. Dejene, H.C. Swart, Phase formation of hexagonal wurtzite ZnO through decomposition of $Zn(OH)_2$ at various growth temperatures using CBD method, Opt. Mater., 46 (2015) 292–298.
[34] P. Liu, W. Cai, J. Chen, Z. Yang, J. Zhou, Z. Cai, J. Fan, One-pot hydrothermal preparation of manganese-doped carbon microspheres for effective deep removal of hexavalent chromium from wastewater, J. Colloid Interface Sci., 599 (2021) 427–435.
[35] J. Lin, L. Wang, Comparison between linear and non-linear forms of pseudo-first-order and pseudo-second-order adsorption kinetic models for the removal of methylene blue by activated carbon, Front. Environ. Sci. Eng. China, 3 (2009) 320–324.
[36] Z. Yin, Y. Liu, S. Liu, L. Jiang, X. Tan, G. Zeng, M. Li, S. Liu, S. Tian, Y. Fang, Activated magnetic biochar by one-step synthesis: enhanced adsorption and coadsorption for 17β-estradiol and copper, Sci. Total Environ., 639 (2018) 1530–1542.
[37] H.K. Boparai, M. Joseph, D.M. O'Carroll, Kinetics and thermodynamics of cadmium ion removal by adsorption onto nano zerovalent iron particles, J. Hazard. Mater., 186 (2011) 458–465.
[38] C. Saucier, M.A. Adebayo, E.C. Lima, R. Cataluña, P.S. Thue, L.D. Prola, M. Puchana-Rosero, F.M. Machado, F.A. Pavan, G. Dotto, Microwave-assisted activated carbon from cocoa shell as adsorbent for removal of sodium diclofenac and nimesulide from aqueous effluents, J. Hazard. Mater., 289 (2015) 18–27.
[39] Y.-S. Ho, G. McKay, Application of kinetic models to the sorption of copper(II) on to peat, Adsorpt. Sci. Technol., 20 (2002) 797–815.
[40] É.C. Lima, M.A. Adebayo, F.M. Machado, Kinetic and Equilibrium Models of Adsorption, C. Bergmann, F. Machado, Eds., Carbon Nanomaterials as Adsorbents for Environmental and Biological Applications, Carbon Nanostructures, Springer, Cham, 2015, pp. 33–69. Available at: https://doi.org/10.1007/978-3-319-18875-1_3
[41] B.S. Marques, T.S. Frantz, T.R. Sant'Anna Cadaval Jr., L.A. de Almeida Pinto, G.L. Dotto, Adsorption of a textile dye onto piaçava fibers: kinetic, equilibrium, thermodynamics, and application in simulated effluents, Environ. Sci. Pollut. Res., 26 (2019) 28584–28592.
[42] Q. Chen, J. Zheng, L. Zheng, Z. Dang, L. Zhang, Classical theory and electron-scale view of exceptional Cd(II) adsorption onto mesoporous cellulose biochar via experimental analysis coupled with DFT calculations, Chem. Eng. J., 350 (2018) 1000–1009.
[43] K.-W. Jung, S.Y. Lee, J.-W. Choi, Y.J. Lee, A facile one-pot hydrothermal synthesis of hydroxyapatite/biochar nanocomposites: adsorption behavior and mechanisms for the removal of copper(II) from aqueous media, Chem. Eng. J., 369 (2019) 529–541.
[44] K. Narasimharao, L.P. Lingamdinne, S. Al-Thabaiti, M. Mokhtar, A. Alsheshri, S.Y. Alfaifi, Y.-Y. Chang, J.R. Koduru, Synthesis and characterization of hexagonal Mg–Fe layered double hydroxide/grapheme oxide nanocomposite for efficient adsorptive removal of cadmium ion from aqueous solutions: isotherm, kinetic, thermodynamic and mechanism, J. Water Process Eng., 47 (2022) 102746, doi: 10.1016/j.jwpe.2022.102746.

[45] C. Bhan, J. Singh, Y.C. Sharma, J.R. Koduru, Synthesis of lanthanum-modified clay soil-based adsorbent for the fluoride removal from an aqueous solution and groundwater through batch and column process: mechanism and kinetics, Environ. Earth Sci., 81 (2022) 253, doi: 10.1007/s12665-022-10377-x.
[46] Y. Bulut, Z. Tez, Adsorption studies on ground shells of hazelnut and almond, J. Hazard. Mater., 149 (2007) 35–41.
[47] A. Özer, D. Özer, The adsorption of copper(II) ions on to dehydrated wheat bran (DWB): determination of the equilibrium and thermodynamic parameters, Process Biochem., 39 (2004) 2183–2191.
[48] M.I. Panayotova, Kinetics and thermodynamics of copper ions removal from wastewater by use of zeolite, Waste Manage., 21 (2001) 671–676.
[49] M. Shafiee, M.A. Abedi, S. Abbasizadeh, R.K. Sheshdeh, S.E. Mousavi, S. Shohani, Effect of zeolite hydroxyl active site distribution on adsorption of Pb(II) and Ni(II) pollutants from water system by polymeric nanofibers, Sep. Sci. Technol., 55 (2020) 1994–2011.
[50] Z. Aksu, İ.A. İşoğlu, Removal of copper(II) ions from aqueous solution by biosorption onto agricultural waste sugar beet pulp, Process Biochem., 40 (2005) 3031–3044.
[51] K. Singh, K. Sarma, A simple and feasible approach to decorating MWCNT with Fe_3O_4 and ZnS and their use as a magnetically separable photocatalyst in the degradation of Cr(VI) in wastewater, Environ. Nanotechnol. Monit. Manage., 6 (2016) 206–213.
[52] M.M. Tehrani, S. Abbasizadeh, A. Alamdari, S.E. Mousavi, Prediction of simultaneous sorption of copper(II), cobalt(II) and zinc(II) contaminants from water systems by a novel multi-functionalized zirconia nanofiber, Desal. Water Treat., 62 (2017) 403–417.
[53] A. Murugesan, T. Vidhyadevi, S.D. Kirupha, L. Ravikumar, S. Sivanesan, Removal of chromium(VI) from aqueous solution using chemically modified corncorb-activated carbon: equilibrium and kinetic studies, Environ. Prog. Sustainable Energy, 32 (2013) 673–680.
[54] C. Yu, M. Wang, X. Dong, Z. Shi, X. Zhang, Q. Lin, Removal of Cu(II) from aqueous solution using Fe_3O_4–alginate modified biochar microspheres, RSC Adv., 7 (2017) 53135–53144.
[55] P. Lin, H. Liu, H. Yin, M. Zhu, H. Luo, Z. Dang, Remediation performance and mechanisms of Cu and Cd contaminated water and soil using Mn/Al-layered double oxide-loaded biochar, J. Environ. Sci., 125 (2023) 593–602.